J. Min. Metall. Sect. B-Metall. 61 (3) (2025) 303 - 315

Journal of Mining and Metallurgy, Section B: Metallurgy

THE INFLUENCE OF COLD, WARM AND HOT DEFORMATION ON MICROSTRUCTURE AND MECHANICAL PROPERTIES OF INCONEL 718 SUPERALLOY

Tugay Doğan, Süleyman Gündüz*, Demet Taştemür

Karabük University, Technology Faculty, Karabük, Türkiye

(Received 29 July 2025; Accepted 17 November 2025)

Abstract

This study systematically examines the influence of precipitation on the microstructural and mechanical properties of Inconel 718 superalloy in as-received, solution heat-treated, peak-aged, and overaged conditions. Cold, warm, and hot deformation tests were performed at 25 °C, 400 °C and 800 °C using a constant strain rate of 5.55×10^{-4} s^{-1}. The results indicated dynamic strain aging during warm deformation at 400 °C in all investigated conditions. However, at temperatures above 400 °C, a pronounced reduction in strength was observed, accompanied by a corresponding increase in elongation for most conditions. Notably, the solution heat-treated samples exhibited anomalous behavior, showing an increase in $Rp_{0.2}$ after deformation at 800 °C. This suggests the occurrence of dynamic precipitation during hot deformation in the solution heat-treated samples.

Keywords: *Superalloys; Dynamic strain aging; Microstructure; Mechanical properties*

1. Introduction

Superalloys, a class of high-performance alloys, are widely employed in applications demanding resistance to elevated temperatures, particularly in the aerospace sector. Inconel 718, a nickel-based superalloy, offers exceptional high-temperature strength, corrosion and oxidation resistance, thermal fatigue resistance, and favorable forgeability and weldability, primarily due to its precipitation hardening behavior [1]. These attributes make it a material of choice for critical engine components such as compressor and turbine disks [2, 3]. Global market research indicates that the aircraft engine market size was approximately 80 billion USD in 2019. Due to the increase in air travel, this figure is expected to exceed 85.4 billion USD by 2027 [4]. More than 50% of an aircraft engine's weight consists of Inconel 718 superalloy [5]. In their research, Pulidindi [6] reported that Inconel 718 accounted for over 54% of the nickel superalloy market share, which exceeded 4 billion USD in 2019, making it the most widely used nickel superalloy worldwide.

The formation of various phases in the Inconel 718 superalloy has been extensively studied leading to the identification of several critical strengthening and secondary phases. These phases include: (a) the γ′ phase ($Ni_3(Al,Ti)$), characterized by a FCC crystal structure; (b) the metastable γ″ phase (Ni_3Nb), possessing a BCT structure; and (c) the equilibrium δ phase (Ni_3Nb) which exhibits an orthorhombic crystal structure. In addition, various carbide phases such as MC, M_6C and $M_{23}C_6$ type carbides, may precipitate during the ageing process at between 600-1050 °C [7]. The γ″ phase precipitates within the matrix over a temperature range of approximately 600 °C to 900 °C, whereas the δ phase typically forms at elevated temperatures ranging from 750 °C to 1020 °C [8]. The transformation of the γ″ phase into the δ phase takes place during heat treatment within the temperature range of 700 °C to 900 °C [9].

Plastic deformation influences the kinetics of precipitates which significantly affect material properties. The properties of alloys depend on the morphologies of precipitates, particularly when subjected to solution treatment or pre-aging. Studies show that alloys subjected to pre-aging at elevated deformation temperatures exhibit reduced strength, primarily as a result of precipitate coarsening. In contrast, solution heat-treated alloys demonstrate higher strength, attributed to increased dislocation density and dynamic precipitation [10, 11]. Microstructural changes caused by plastic deformation at elevated temperatures and aging significantly influence mechanical properties across various temperature ranges. Studies show that aging

Corresponding author: sgunduz@karabuk.edu.tr

https://doi.org/10.2298/JMMB250729024D

CC BY SA

treatments improve hardness and tensile strength, while prolonged aging reduces impact strength and tensile ductility [12]. In Ni-based superalloys, serrated flow behavior observed in the stress-strain response at elevated temperatures is attributed to the phenomenon known as dynamic strain aging (DSA). These serrations observed on the stress-strain diagrams due to interaction between dislocations and solute atoms [13, 14].

In the literature, investigating thermomechanical and heat treatment processes of Inconel 718 superalloy is of great importance. Consequently, there is a need to further expand the application areas of these alloys. By systematically correlating the deformation regime with precipitation behavior and strength, the paper offers novel insights into how hot deformation history can be optimized to tailor performance in service environments. This integrated approach bridges a critical gap in the literature, where the combined effects of deformation temperature and aging on precipitation kinetics and mechanical response have remained comparatively underexplored. This study has been carried out to address these needs and to establish the optimal relationship between microstructure and mechanical properties in these alloys. In addition, tensile deformation investigations conducted at elevated temperatures show that DSA occurs in Inconel 718 superalloy, accompanied by a shift from planar to wavy slip as the ageing duration increases. These findings are assessed to evaluate the effect of different microstructures on cold, warm, and hot deformation behavior.

2. Materials and methods

The material utilized in the current experimental study is Inconel 718, a high performance superalloy selected to investigate its deformation behavior under various heat-treated conditions. Specifically, the study evaluates the deformation behavior under cold, warm, and hot conditions in the as-received (A1), solution heat-treated (A2), peak-aged (A3), and overaged (A4) microstructural states. The elemental composition of Inconel 718 is provided in Table 1. The tensile test samples were prepared in accordance with the ASTM E8 standard.

The tensile samples, excluding those in the A1 condition, were heat-treated at 1050 °C for 2 h, followed by water quenching to attain a supersaturated solution. A subset of the A2 samples was subsequently subjected to aging at 810 °C for 8 h, whereas another subset underwent ageing at the same temperature for an 80 h. Figure 2 shows schematic presentation of heat treatment process. These ageing times were chosen to represent the A3 and A4 conditions. The A1, A2, A3, and A4 samples were subjected to tensile testing at a constant strain rate of 5.55×10^{-4} s^{-1} and temperatures of 25 °C, 400 °C and 800 °C utilizing a universal testing machine with a 100 kN load capacity. Engineering stress-strain curves were obtained for each test condition, from which the ultimate tensile strength (R_m), 0.2% offset yield strength ($Rp_{0.2}$), elongation (%), and the increase in strength resulting from work hardening (δy) were subsequently evaluated.

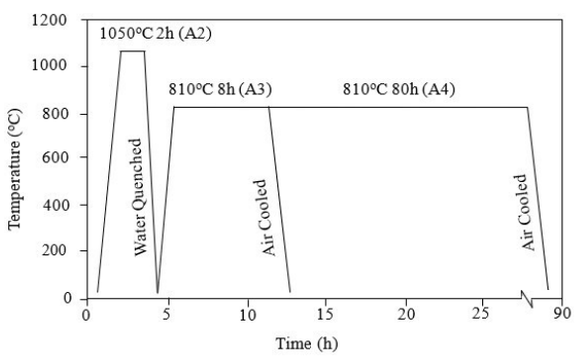

Figure 1. *Schematic presentation of heat treatment process*

Microstructural characterization of the Inconel 718 superalloy was conducted using optical microscopy and SEM. This characterization was carried out on A1, A2, A3 and A4 samples following mechanical testing at 25 °C, 400 °C and 800 °C. The samples were initially ground using silicon carbide abrasive papers, followed by polishing with diamond suspension to obtain a scratch free surface suitable for microstructural examination. To reveal the microstructure, all samples were etched using a solution composed of 2 ml nitric acid (HNO_3), 2 ml hydrochloric acid (HCl) and 1 ml hydrofluoric acid (HF).

3. Results and discussion

Figure 2(a) and Figure 3(a) illustrate the optical and SEM microstructure of Inconel 718 superalloy in the as-received (A1) condition, revealing an austenitic matrix composed of equiaxed grains accompanied by finely dispersed precipitates. Following solution heat treatment (A2) conducted at 1050 °C for 2 h, the precipitates dissolved and entered into the solid solution, reducing their quantity (Figure 2(b) and Figure 3(b)). In the peak-aged (A3) condition,

Table 1. *Elemental composition of Inconel 718*

Elements	C	Si	Mn	P	S	Cr	Mo	Cu	Co	Ti	Al	Nb	Ni
(wt%)	0.024	0.06	0.09	0.008	0.003	17.75	2.98	0.06	0.34	0.99	0.54	5.17	bal.

CC BY SA

uniformly distributed precipitates ranging from small to medium in size were observed (Figure 2(c) and Figure 3(c)), significantly enhancing the alloy's strength [15]. Further aging led to the dissolution of smaller precipitates, reducing their number, while overaging (A4) resulted in the formation of larger precipitates (Figure 2(d) and Figure 3(d)). This coarsening phenomenon has been extensively reported and documented in the literature [16].

Figure 3 presents the results of EDS line scan analysis conducted on the A4 samples tested at ambient temperature. Elemental distribution profiles of Ni, Nb, and Mo along the scanned line are depicted in Figure 3(e), revealing two distinct phases: a Ni enriched matrix and a Nb and Mo enriched precipitate phase. Nb and Mo exhibited a pronounced increase in concentration from the Ni-rich matrix toward the precipitate, whereas Ni displayed an inverse trend. In light of both the present findings and relevant literature, the presence and distribution of these elements suggest the formation of γ″ phase, δ phase and Mo_6C carbides during the overaging process.

Figure 4 illustrates the evolution of precipitates in A2 samples subjected to testing at 25 °C, 400 °C, and 800 °C. Figure 4(a) depicts precipitates occurred under static conditions, whereas Figures 4(b) and 4(c) present precipitates developed dynamically during deformation. These results indicate that precipitation occurred and progressed through coarsening with increasing test temperature. Microstructural analysis revealed the formation of fine, complex or spheroidal precipitates ranging from 1 to 5 μm within the grains following testing at 400 °C. Upon increasing testing temperature to 800 °C, both the size and volume fraction of these complex or spheroidal precipitates were observed to increase, as shown in Figure 4(c). Similar observations have been reported in previous studies investigating dynamic precipitation behavior in Inconel 718 superalloy [16, 17]. Point EDS analysis was conducted on the A2 samples subjected to tensile testing at 400 °C, as shown in Figure 4(d). The elemental composition analysis revealed that points 1 and 3 contain Nb, Ti, and C; point 2 is composed of Nb, Ni, Cr and C; points 4 and 6–8 exhibit the presence of Nb, Mo, Ni, Cr and C; while point 5 consists of Nb, Ni, Cr and C. The detection of these elements suggests the formation of the γ′ phase, the metastable γ″ phase, the equilibrium δ phase and MC

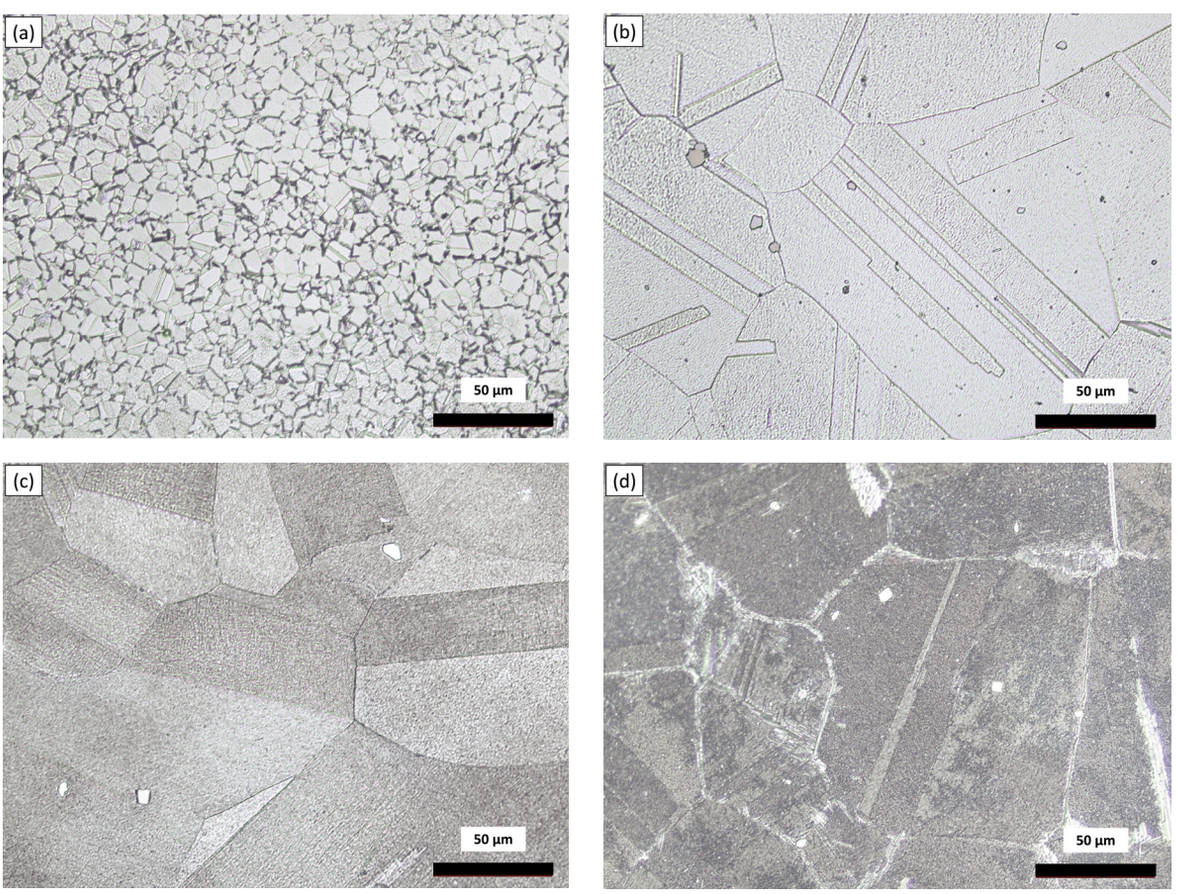

Figure 2. *Bright field optical microstructures of Inconel 718 superalloy samples subjected to tensile testing at room temperature: (a) A1, (b) A2, (c) A3 and (d) A4 samples*

CC BY SA

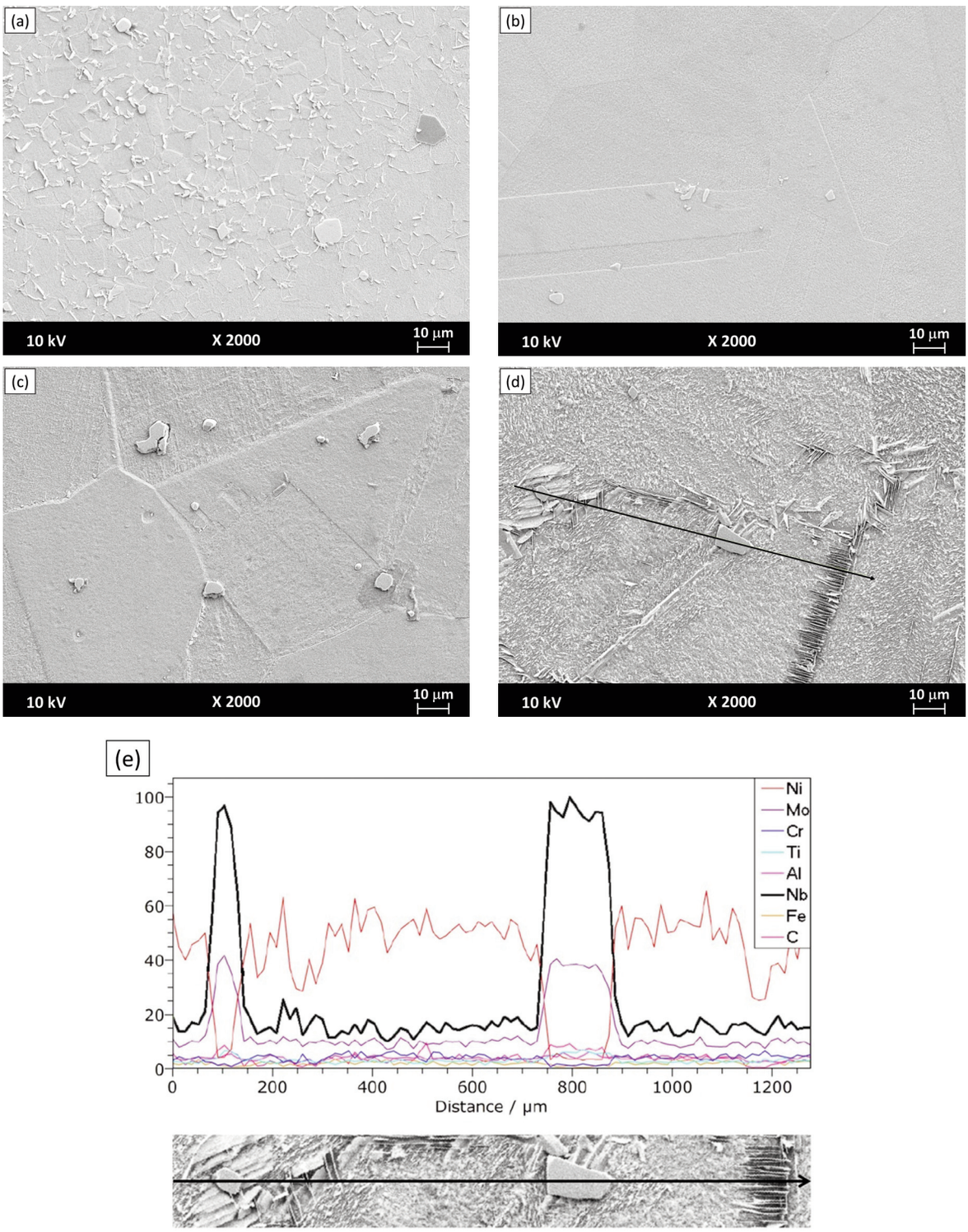

Figure 3. *SEM microstructures of Inconel 718 superalloy samples subjected to tensile testing at room temperature: (a) A1, (b) A2, (c) A3, (d) A4 samples and (e) line scan EDS analysis of the over aged condition*

type precipitates such as $Cr_{23}C_6$, Mo_6C and Nb,Ti(C) in the Inconel 718 superalloy under A2 conditions following high temperature deformation, consistent with the findings reported by Peikang et al. [18]. These precipitate particles can significantly affect the properties of the Inconel 718 superalloy by enhancing

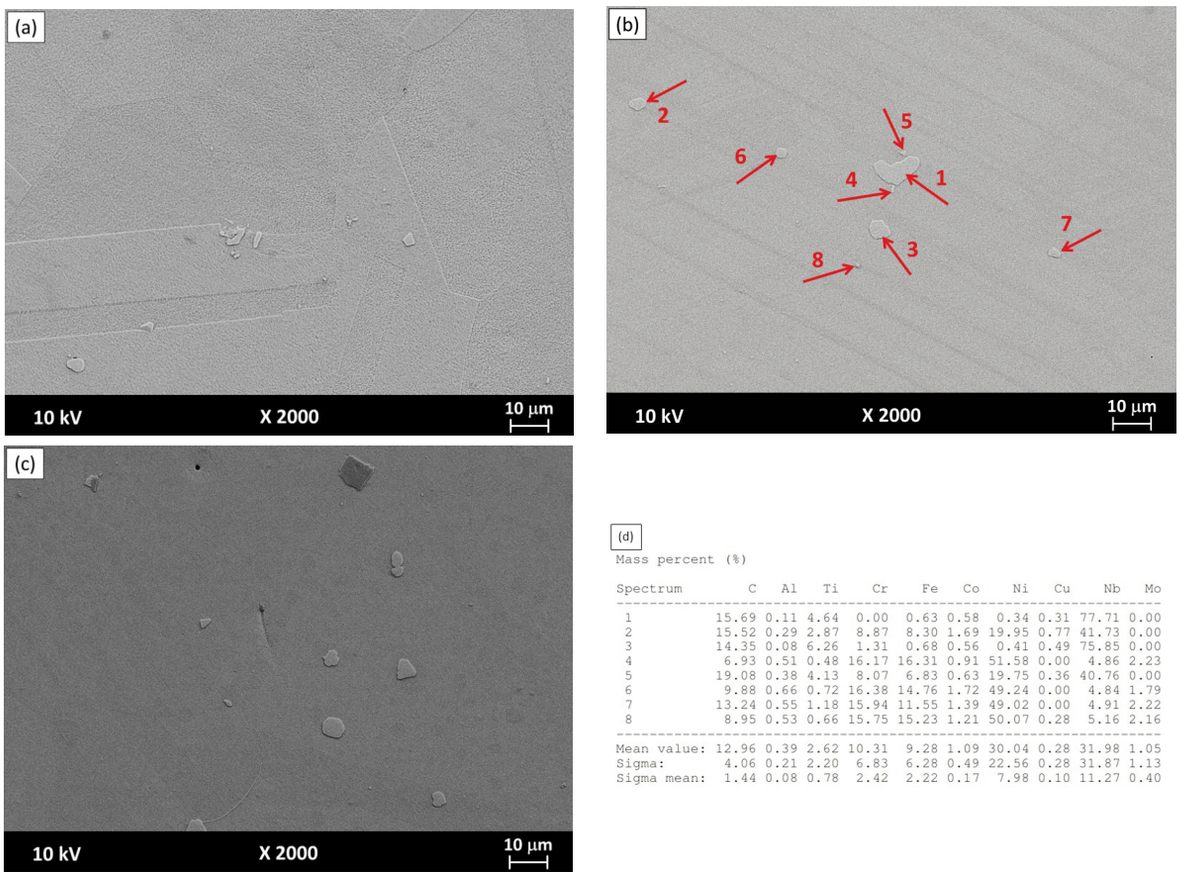

Figure 4. *Microstructures of A2 samples following mechanical testing at (a) 25 °C, (b) 400 °C and (c) 800 °C and (d) EDS analysis of the A2 sample tested at 400 °C*

yield strength through mechanisms such as dislocation-dislocation interactions and dislocation-precipitate interactions.

Figure 5 presents the properties of Inconel 718 superalloy in the A1, A2, A3 and A4 conditions. The A1 samples revealed a R_m of 1463 MPa and a $Rp_{0.2}$ of 1414 MPa. In contrast, the A2 samples demonstrated the lowest strength, with a R_m of 787 MPa and a $Rp_{0.2}$ of 332 MPa, following heat treatment at 1050 °C for 2 h and subsequent water quenching. An enhancement in both R_m and $Rp_{0.2}$ was observed in the A3 samples following ageing at 810 °C for 8 h. However, extending the ageing duration to 80 h at the same temperature resulted in a reduction in R_m and $Rp_{0.2}$ in the A4 samples. It was further noted that the A1 samples exhibited a percentage elongation of 10%. This value significantly increased to 53% (the highest observed) following solution heat treatment of A2 samples. The A3 samples, aged at 810 °C for 8 h, demonstrated intermediate ductility with an elongation of 19%. A slight increase in elongation to 20% was observed in the A4 samples after ageing at 810 °C for 80 h. Variations in strength and ductility of Inconel 718 can be attributed to the formation of distinct precipitate phases, including the γ′ phase, the metastable γ″ phase and the equilibrium δ phase [7]. During artificial ageing, the γ′ and γ″ phases begin to precipitate, with their volume fractions increasing as ageing time progresses. This precipitation enhances the strength of the Inconel 718 superalloy while reducing its ductility. However, prolonged ageing promotes the formation of coarser δ phase precipitates, which results in a reduction in strength but a corresponding increase in percentage elongation [2, 19]. Piotr et al. [20] reported that ageing at 650 °C -750 °C leads to peak strength; however, extended ageing times results in property degradation due to precipitate coarsening. Similarly, Slama et al. [21] demonstrated that over ageing reduces hardness because of the loss of coherent strengthening precipitates.

Figure 5 also presents the test results of Inconel 718 superalloy at 25 °C, 400 °C and 800 °C under A1, A2, A3 and A4 conditions. Both Rm and $Rp_{0.2}$ of the A1, A3, and A4 samples exhibited a progressive decline with increasing temperature across the range of 25–800 °C. However, the A2 samples exhibited an increment in $Rp_{0.2}$ when tested at 800 °C. This

CC BY SA

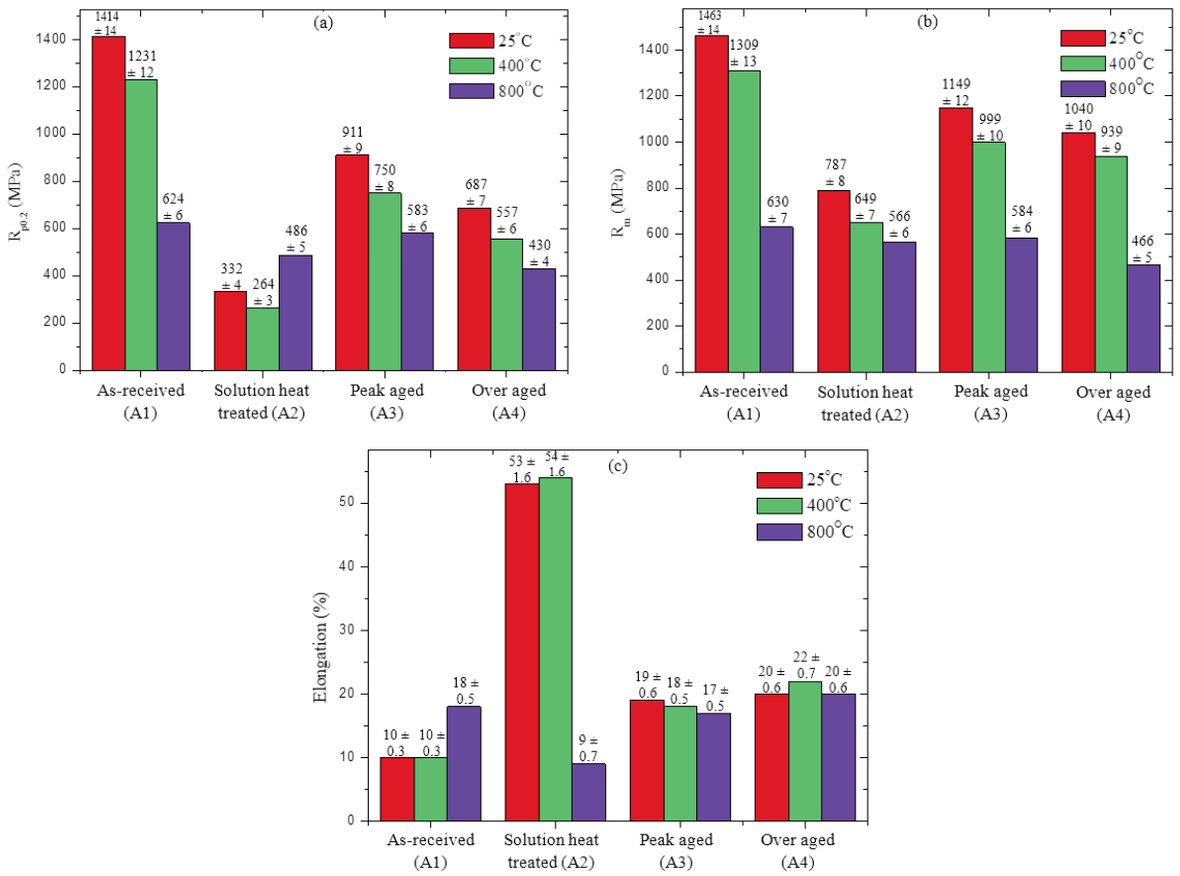

Figure 5. *(a) $Rp_{0.2}$, (b) R_m and (c) percentage elongation values of Inconel 718 samples tested at various temperatures*

behavior is attributed to dynamic precipitation occurring during high temperature tensile testing at 800 °C, which lies within the optimal precipitation range of the γ″ phase. The dynamic precipitation is facilitated by deformation-induced nucleation and enhanced atomic diffusion under these thermal and mechanical conditions. These results are consistent with the findings reported by Zhang et al. [22] and Theska et al. [23] who demonstrated that fine γ″ precipitates preferentially form along dislocation lines and subgrain boundaries because of plastic deformation at 800 °C. They concluded that dynamic precipitation contributes to impede dynamic recrystallization by exerting a pinning effect on grain and subgrain boundaries. Dynamic precipitation in solution heat-treated Inconel 718 superalloy during hot tensile testing at 800 °C is characterized by the accelerated formation of γ″ precipitates (along with limited formation of γ′ and δ phases) facilitated by strain-enhanced atomic diffusion and dislocation-assisted nucleation mechanisms. This phenomenon exerts a pronounced influence on both the mechanical behavior and microstructural evolution of the alloy, thereby representing a critical consideration in the design of hot deformation processing routes. As evidenced by the preceding analysis, the dynamic precipitation of γ″ during deformation contributes to enhanced strength retention, even under elevated temperature conditions. However, the R_m for the same sample continues to decrease from 787 MPa at 25 °C to 566 MPa at 800 °C. This is due to thermal softening, precipitate coarsening and dynamic recovery which limit further strengthening, so the material fails at a lower stress than might be expected. Also, at 800 °C dislocations can move and rearrange easily, therefore the material cannot significantly strengthen after initial yielding, so R_m remains low [24, 25].

A progressive increase in elongation was also observed in the A1, A3 and A4 samples with increasing test temperature up to 800 °C. This behavior is attributed to the occurrence of dynamic recovery and recrystallization processes, which progressively reduce the constraints on grain boundary mobility present at room temperature, thereby enhancing ductility at elevated temperatures. In contrast to the A1, A3 and A4 samples, the A2 samples exhibited a reduction in elongation with increasing test temperature up to 800 °C, indicating an inverse trend in ductility behavior under elevated

CC BY SA

temperature conditions. It is well established that A2 samples retain higher concentrations of Ni, Al, Ti and Nb in solid solutions because of the rapid cooling rate associated with solution heat treatment, which limits the time available for the formation of equilibrium precipitates. Extensive studies have demonstrated that elevated cooling rates following solution heat treatment (such as those achieved by water quenching) effectively suppress the diffusion-controlled precipitation of strengthening phases. Consequently, alloying elements such as Ni, Al, Ti and Nb, which would otherwise participate in the formation of γ′ and δ precipitates during slower cooling processes, predominantly remain in solid solution [26, 27]. However, during hot tensile testing at 800 °C, the A2 samples underwent dynamic precipitation, resulting in an increment in strength accompanied by a reduction in elongation. For instance, the A2 samples exhibited an approximate 46% enhancement in $Rp_{0.2}$ at a testing temperature of 800 °C compared to those tested at 25 °C. This pronounced enhancement in strength indicates the significant contribution of dynamic precipitation in the A2 condition under high temperature deformation. Also, short-range order or clustering effects in the matrix can momentarily increase resistance to dislocation motion. This gives a high initial yield strength [24, 25].

Figure 6 presents the engineering stress–strain curves of A2 samples tested at 25 °C, 400 °C and 800 °C under a 5.55×10^{-4} s^{-1} strain rate. As seen from Figure 5 that the A2 samples tested at 400 °C exhibited serrated flow behavior, characteristic of the PLC effect. The underlying mechanism of PLC in Inconel 718 is attributed to dynamic strain aging, arising from the interaction between dislocations and solute atoms, primarily Ni, Nb, and C, which remain in solid solution following the solution heat treatment. At elevated temperatures such as 400 °C, the diffusion rates of solute atoms increase significantly, enabling

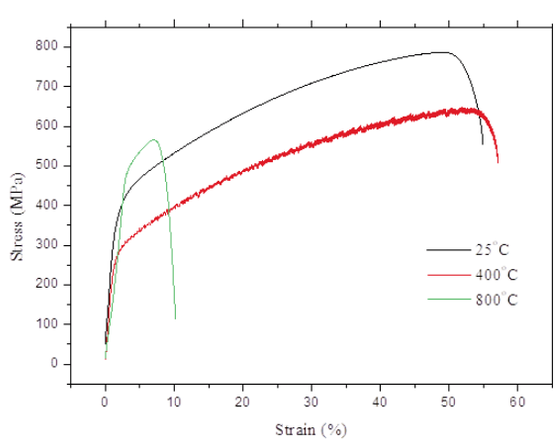

Figure 6. *Engineering stress–strain curves of A2 samples evaluated at various testing temperatures*

them to interact more readily with mobile dislocations. This interaction leads to the temporary pinning of dislocations, resulting in the characteristic serrated or jerky appearance of the stress-strain curve, which arises from the repeated pinning and unpinning of dislocations during plastic deformation [28, 29].

Literature studies [30, 31] have reported the occurrence of different types (A, B and C) PLC deformation bands in superalloys, each distinguished by their dynamic characteristics. As illustrated in Figure 6, the stress–strain response of the A2 samples subjected to testing at 400 °C exhibits feature indicative of a type-B PLC effect. Type-B serrations, characterized by rapid and successive oscillations superimposed on the overall stress–strain curve, arise from the intermittent nucleation of localized deformation bands. These bands typically initiate at non-propagating or sporadically propagating peak stresses and are followed by the formation of additional bands either in adjacent regions or at a distance from the initial site. Type-B serrations can evolve from type-A serrations at higher stress levels or may manifest directly during plastic deformation at elevated temperatures and lower strain rates, relative to the conditions associated with type-A behavior. In practical applications, a combination of type-A and type-B serrations may be observed concurrently, resulting in a mixed-mode serrated flow behavior [28, 32]. This phenomenon can be ascribed to the intensified interaction between dislocations and precipitates, Ni clusters, or solute atoms at 400 °C.

In this study, the PLC effect was also detected in the A1, A3, and A4 samples following tensile testing at 400 °C (see Figure 7). This behavior indicates a different concentration of free Ni, Al, Ti, and Nb atoms retained in the solution of the A1, A2, A3 and A4 samples depending on the heat treatment conditions. The serrated flow behavior in Inconel 718 is closely associated with the amount of solute atoms present in the γ matrix. As the concentration of solute atoms increases, dislocation pinning by diffusing solute atoms becomes more prominent, resulting in enhanced serration intensity and frequency in the stress-strain curve.

At moderate solute concentrations, DSA is maximized, leading to pronounced serrated behavior. However, when the solute content reaches levels where precipitate nucleation and growth begin (e.g., γ′/γ″ formation during aging), the availability of solute atoms for dislocation pinning decreases. Consequently, serrated flow becomes weaker and may eventually disappear in overaged conditions, where significant precipitation and coarsening limit solute mobility [33, 34]. As also seen in Figure 7 that solution heat-treated A2 sample exhibits serrated behaviour with high ductility at 400 °C, since γ′/γ″ precipitates have not yet formed. Due to dynamic

CC BY SA

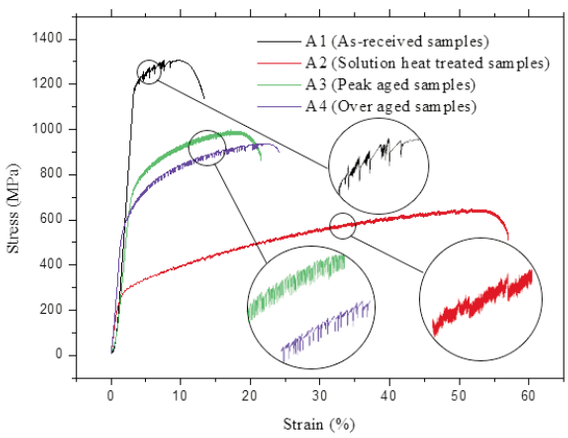

Figure 7. *Engineering stress–strain curves of A1, A2, A3 and A4 samples evaluated at 400 °C*

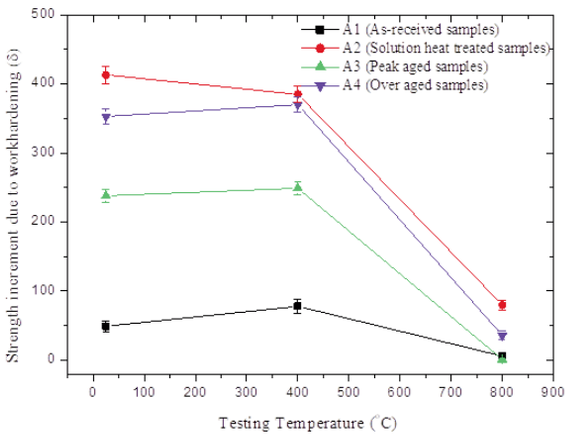

Figure 8. *The increase in strength is attributed to work hardening (δy) in A1, A2, A3 and A4 samples*

strain aging mechanisms, it shows more pronounced serrated flow behavior compared to peak-aged A3 and overaged A4 samples. In peak-aged samples, these effects diminish, and in the overaged condition, the reduction becomes even more due to precipitation of γ′/γ″ phase.

The significantly more pronounced serrated flow behavior observed in A2 sample, compared to samples A1, A3, and A4 samples, indicates a much higher amount of solute atoms but fewer precipitate particles, which are not sufficiently strong to produce a net increase in work hardening. During testing at 800 °C, these solute atoms dynamically precipitated, thereby increasing the $Rp_{0.2}$ strength of A2 sample.

The increase in strength resulting from work hardening (δy) was quantified for the A1, A2, A3 and A4 samples to assess the extent of the PLC effect, which a mechanism referred to as DSA [35]. Work hardening contribution to strength was quantified by subtracting $Rp_{0.2}$ values from R_m values for the A1, A2, A3 and A4 samples, under uniaxial tensile testing conducted at 25 °C, 400 °C, and 800 °C, as illustrated in Figure 8.

The increase in strength resulting from work hardening in the A2 samples exhibited a decreasing trend with increasing test temperature, particularly at 400 °C. In contrast, the increase in strength attributable to work hardening of the A1, A3 and A4 samples exhibited a slight increase at 400 °C, followed by a reduction as the test temperature was further increased to 800 °C. The reason why the solution heat-treated A2 sample exhibits a decrement in strength resulting from work hardening at 400 °C is that there are not enough precipitate obstacles in its microstructure, allowing dislocations to move and rearrange easily at this temperature (dynamic recovery) [26].

Figure 9 presents the SEM fractographic analysis of the A1, A2, A3 and A4 samples tested at 25 °C. The A2 samples exhibited a transgranular fracture mode characterized by micro void coalescence, as evidenced by the presence of dimpled surface morphology (Figure 9b). This fracture morphology is indicative of the high elongation observed prior to failure [36]. In contrast, the A1 and A3 samples aged at 810 °C for 8 h exhibited a mixed fracture mode, with the coexistence of dimples and cleavage facets evident in Figures 9a and 9c. This observation aligns with the elongation data of the A1 and A3 samples, both of which demonstrated the lowest ductility among the tested conditions. The reduced elongation is attributed to embrittlement arising from the interaction between dislocations and precipitates [37]. Prolonged ageing at 800 °C for 80 h led to a greater prevalence of dimpled fracture features on the surface of the A4 samples (Figure 9d), accompanied by an increase in elongation. This behavior is attributed to the coarsening of precipitate particles along dislocation lines, which facilitated enhanced ductility. The A4 samples also exhibited prominent deep cusps on the fracture surface, attributed to the detachment of coarsened precipitates from the matrix, induced by the application of tensile loading. Precipitate particles were identified on the fracture surfaces of the A1, A2, A3 and A4 samples. For instance, point EDS analysis of the A3 samples revealed the presence of complex Ni–Al–Nb–Ti–Cr–Mo precipitates (Figure 9e).

Figure 10 presents the SEM fractography of A2 samples tested at 25°C, 400°C and 800°C. The fracture surfaces of the A2 sample exhibited a combination of dimples and cleavage facets across all testing temperatures, as shown in Figures 10a–c. Conversely, the A2 samples exhibited a transition from ductile transgranular features to intergranular fracture zones as the testing temperature was elevated from 25°C to 400°C and 800°C. This is due to grain boundary weakening and coarsening of precipitates such as γ′, γ″ and MC type precipitates such as $Cr_{23}C_6$, Mo_6C and Nb,Ti(C) which can form in Inconel 718 superalloy as a function of the applied heat treatment

CC BY SA

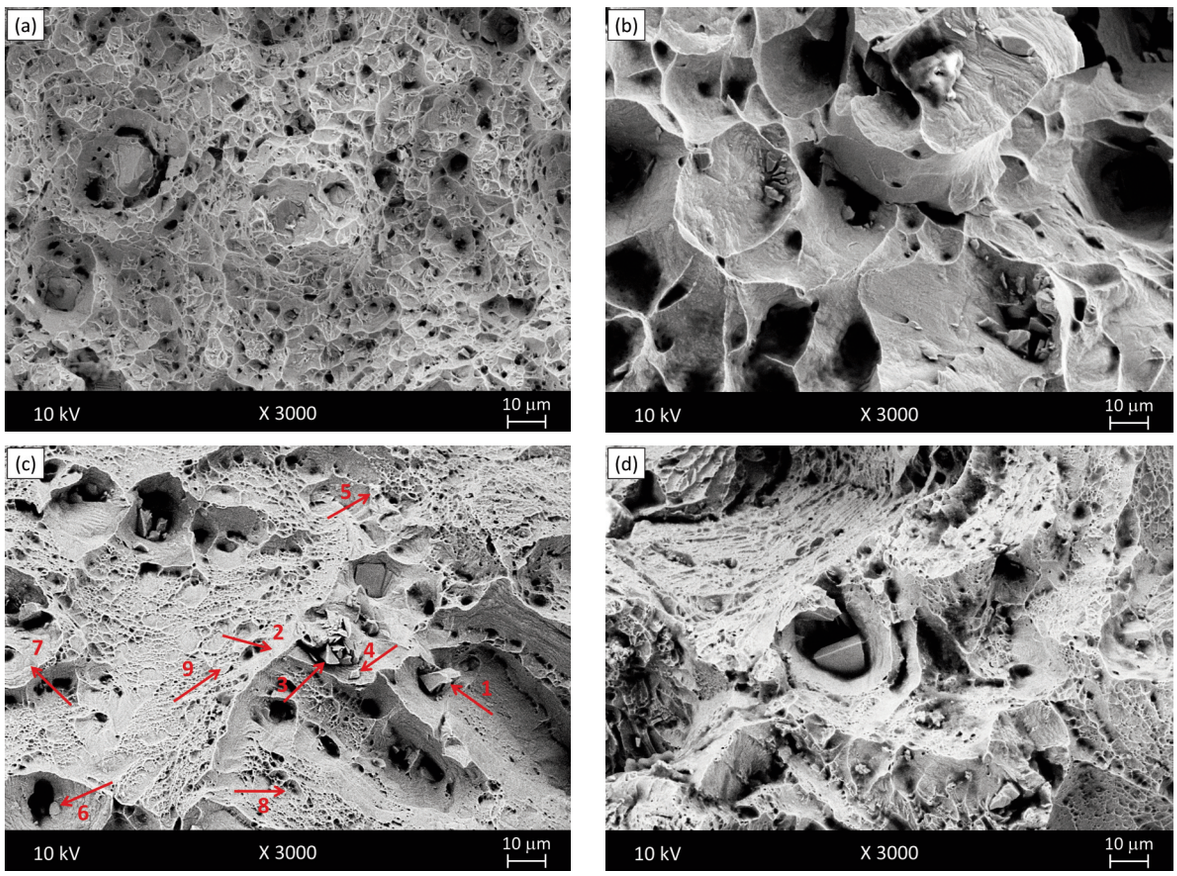

(e)

Mass percent (%)

Spectrum	C	Al	Ti	Cr	Fe	Co	Ni	Cu	Nb	Mo
1	16.09	0.11	3.93	10.42	11.93	0.62	14.97	0.29	41.64	0.00
2	14.07	0.73	0.62	12.29	11.24	1.63	52.12	1.48	4.22	1.59
3	12.97	0.17	1.57	22.55	21.98	0.83	31.90	0.00	6.41	1.62
4	6.84	0.28	2.94	25.26	21.96	1.23	34.92	0.53	4.76	1.29
5	10.30	0.65	1.03	14.94	11.66	2.00	50.89	1.87	4.65	2.02
6	17.69	0.41	0.47	13.06	12.39	2.27	46.85	0.74	3.97	2.15
7	8.47	0.59	0.46	13.22	13.31	2.72	53.50	0.65	4.90	2.18
8	16.43	0.65	0.81	12.04	11.46	1.48	50.02	0.59	4.84	1.67
9	14.79	0.67	0.64	14.05	11.38	1.60	49.88	0.72	4.44	1.82
Mean value:	13.07	0.47	1.38	15.32	14.14	1.60	42.78	0.76	8.87	1.59
Sigma:	3.76	0.24	1.24	5.08	4.48	0.67	12.95	0.57	12.31	0.66
Sigma mean:	1.25	0.08	0.41	1.69	1.49	0.22	4.32	0.19	4.10	0.22

Figure 9. *Fracture surfaces of (a) A1, (b) A2, (c) A3 and (d) A4 samples tested at 25 °C, along with (e) point EDS analysis of the precipitates*

and cooling rate [38]. Also, the solution heat-treated structure is weaker than the aged microstructure in terms of oxidation resistance and thermal stability. During deformation of the A2 samples at 400°C and 800°C, oxidation may develop along the grain boundaries, which facilitates crack propagation and increases brittleness [39]. Point EDS analysis confirmed the presence of complex Ni–Al–Nb–Ti–Cr–Mo–rich precipitate phases in the A2 samples, as illustrated in Figure 10d.

CC BY SA

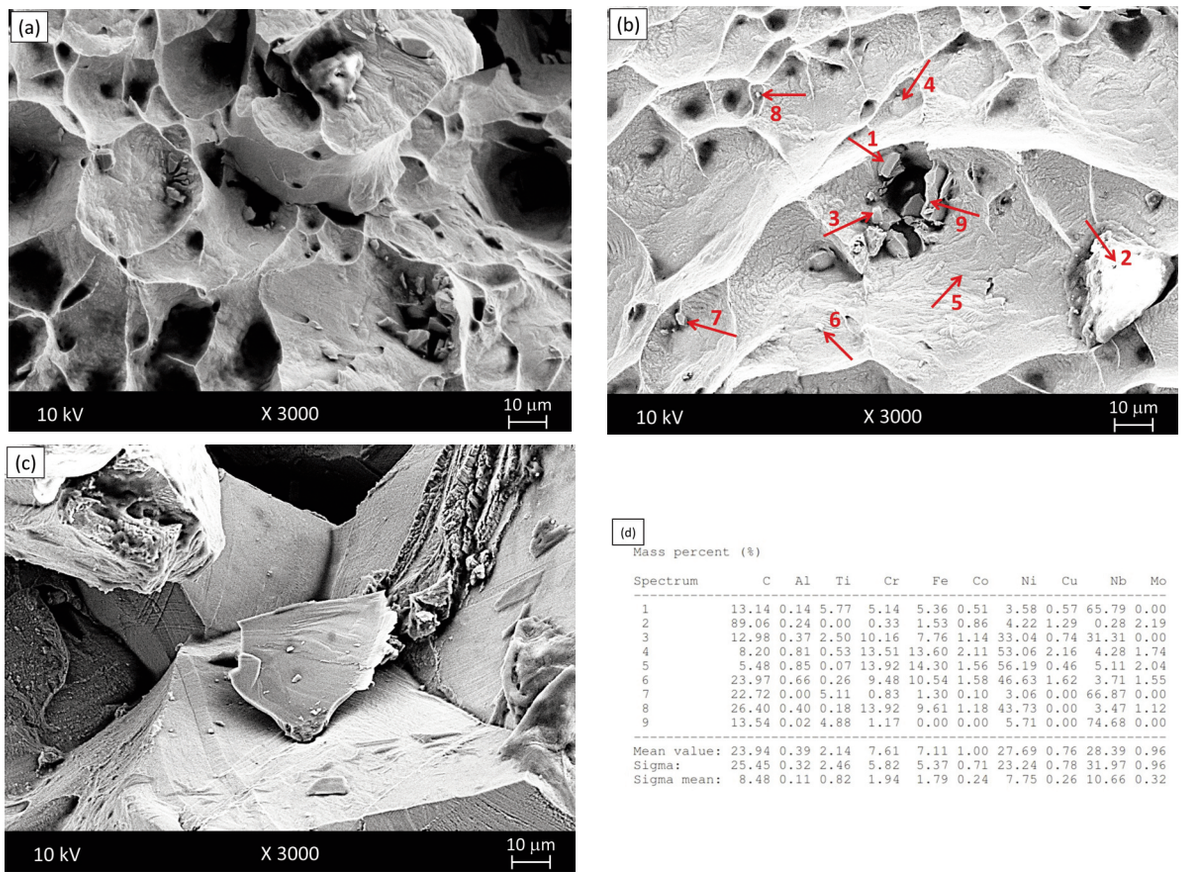

Spectrum	C	Al	Ti	Cr	Fe	Co	Ni	Cu	Nb	Mo
1	13.14	0.14	5.77	5.14	5.36	0.51	3.58	0.57	65.79	0.00
2	89.06	0.24	0.00	0.33	1.53	0.86	4.22	1.29	0.28	2.19
3	12.98	0.37	2.50	10.16	7.76	1.14	33.04	0.74	31.31	0.00
4	8.20	0.81	0.53	13.51	13.60	2.11	53.06	2.16	4.28	1.74
5	5.48	0.85	0.07	13.92	14.30	1.56	56.19	0.46	5.11	2.04
6	23.97	0.66	0.26	9.48	10.54	1.58	46.63	1.62	3.71	1.55
7	22.72	0.00	5.11	0.83	1.30	0.10	3.06	0.00	66.87	0.00
8	26.40	0.40	0.18	13.92	9.61	1.18	43.73	0.00	3.47	1.12
9	13.54	0.02	4.88	1.17	0.00	0.00	5.71	0.00	74.68	0.00
Mean value:	23.94	0.39	2.14	7.61	7.11	1.00	27.69	0.76	28.39	0.96
Sigma:	25.45	0.32	2.46	5.82	5.37	0.71	23.24	0.78	31.97	0.96
Sigma mean:	8.48	0.11	0.82	1.94	1.79	0.24	7.75	0.26	10.66	0.32

Figure 10. *Fracture surfaces of A2 samples tested at (a) 25 °C, (b) 400 °C and (c) 800 °C, (d) point EDS analysis of the indicated precipitates on the fracture surface*

4. Conclusion

In this study, the influence of precipitation on the deformation behavior of Inconel 718 superalloy was systematically investigated under A1, A2, A3 and A4 conditions. Uniaxial tensile tests were conducted at temperatures of 25 °C, 400 °C and 800 °C under a constant strain rate of 5.55×10^{-4} s^{-1}. The corresponding results are summarized as follows.

1. In the as-received (A1) condition, Inconel 718 superalloy exhibited an austenitic matrix composed of equiaxed grains with finely dispersed precipitates. After solution heat treatment (A2), the precipitates dissolved into the solid solution, reducing their quantity. In the peak-aged condition (A3), uniformly distributed precipitates ranging from small to medium size were observed, significantly enhancing the alloy's strength. Further aging led to the dissolution of smaller precipitates, reducing their number, while overaging (A4) resulted in the formation of larger precipitates.

2. The $Rp_{0.2}$ of the A1, A3, and A4 samples showed a continuous decline with increasing test temperature from 25 °C to 400 °C and 800 °C. In contrast, A2 samples exibited an increase in $Rp_{0.2}$ as the test temperature was raised to 800 °C. This enhancement suggests a more pronounced occurrence of dynamic precipitation in the A2 samples under elevated temperature deformation. However, the R_m for the same sample continued to decrease as the test temperature increased to 800°C. This is due to thermal softening, precipitate coarsening, and dynamic recovery, which limit further strengthening, causing the material to fail at a lower stress than might be expected.

3. SEM fractographic analysis revealed that the A2 samples exhibited a transgranular fracture characterized by microvoid coalescence, evidenced by the presence of dimples, after testing at 25 °C. However, the fracture surfaces of A1 and A3 samples subjected to aging at 810 °C for 8 h. exhibited a combination of dimples and cleavage facets. Prolonging the aging duration to 80 h at the same temperature led to an increased prevalence of dimpled morphology on the A4 samples, indicating enhanced ductile fracture characteristics.

4. The fracture surfaces of A2 samples tested at 25 °C, 400 °C and 800 °C exhibited a mixed-mode

CC BY SA

fracture characterized by both dimples and cleavage facets. Conversely, the A2 samples showed a transition from ductile transgranular features to intergranular fracture zones as the testing temperature increasede from 25 °C to 400 °C and 800 °C. This is due to grain boundary weakening and coarsening of precipitates.

Acknowledgments

This study was supported by Scientific and Technological Research Council of Turkey (TUBITAK) under the Grant Number 124M740. The authors thank to TUBITAK for their supports.

Author's contributions

T. Doğan: Conceptualization, Methodology, Investigation, Data analysis, Writing – original draft.
S. Gündüz: Investigation, Data analysis, Discussion, Writing – original draft.
D. Taştemür: Conceptualization, Methodology, Investigation, Data analysis, Writing – original draft.

Data Availability

The data that support the findings of this study are available from the corresponding author, Süleyman Gündüz, upon reasonable request.

Conflict of interest

On behalf of all authors, the corresponding author states that there is no conflict of interest.

References

[1] K. Subramanian, H.P. Cherukuri, Microstructural modeling during multi-pass rolling of a nickel-base superalloy, Proceedings of ASME 2009 International Mechanical Engineering Congress and Exposition (IMECE2009), November 13-19, Lake Buena Vista, Florida, USA, 2009, p.71-73.

[2] Z. İnanır, Effects of high temperature on the structural and mechanical properties of solution treated and aged Inconel 718 alloys), Master's thesis, Istanbul Technical University, Institute of Science, 2012. (in Turkish)

[3] C.M. Kuo, Y.T. Yang, H.Y. Bor, C.N. Wei, C.C. Tai, Aging effects on the microstructure and creep behavior of Inconel 718 superalloy, Materials Science and Engineering: A, 510-511 (2009) 289-294. https://doi.org/10.1016/j.msea.2008.04.097

[4] M. Mazareanu, Aircraft engine market size worldwide 2019–2027, Statista, 2021. https://www.statista.com/statistics/1100610/aircraft-engine-market-sizeworldwide/

[5] D. Ulutan, T. Ozel, Machining induced surface integrity in titanium and nickel alloys: a review, International Journal of Machine Tools and Manufacture, 51 (3) (2011) 250–280. https://doi.org/10.1016/j.ijmachtools.2010.11.003

[6] K.E. Pulidindi, Nickel superalloy market size, by type (Alloy 600/601/602, Alloy 625, Alloy 718, Alloy 825, Alloy 925, Hastelloy C276/C22/X, Waspaloy), by shape (bar, wire, sheet & plate), by application (aerospace & defense, power generation, oil & gas, refinery, chemical), Global Market Insights, 2020. https://www.gminsights.com/industry-analysis/nickel-superalloy-market.

[7] Y. Huang, T.G. Langdon, The evolution of delta-phase in a superplastic Inconel 718 alloy, Journal of Materials Science, 42 (2007) 421–427. https://doi.org/10.1007/s10853-006-0483-z

[8] S. Azadian, L.Y. Wei, R. Warren, Delta phase precipitation in Inconel 718, Materials Characterization, 53 (1) (2004) 7-16. https://doi.org/10.1016/j.matchar.2004.07.004

[9] Y.C. Lin, J. Deng, Y.Q. Jiang, D.X. Wen, G. Liu, Effects of initial δ phase on hot tensile deformation behaviors and fracture characteristics of a typical Ni-based superalloy, Material Science and Engineering: A, 598 (2014) 251-262. https://doi.org/10.1016/j.msea.2014.01.029

[10] J.D. Seidt, A. Gilat, Plastic deformation of 2024-T351 aluminum plate over a wide range of loading conditions, International Journal of Solids and Structures, 50 (10) (2013) 1781–1790. https://doi.org/10.1016/j.ijsolstr.2013.02.006

[11] A. Coşkun, S. Gündüz, An investigation on cold, warm and hot deformation behaviour of Al 2024 alloy under as-received, solution heat treated, peak aged and over aged conditions, Canadian Metallurgical Quarterly, 59 (3) (2020) 297–305. https://doi.org/10.1080/00084433.2020.1757995

[12] A.H.V. Pavan, R.L. Narayan, S.-H. Li, K. Singh, U. Ramamurty, Mechanical behavior and dynamic strain ageing in Haynes® 282 superalloy subjected to accelerated ageing, Materials Science and Engineering: A, 832 (2022) 142486. https://doi.org/10.1016/j.msea.2021.142486

[13] R. Zhang, C. Tian, C. Cui, Y. Zhou, X. Sun, Portevin-Le Châtelier effect in a wrought Ni–Co based superalloy, Journal of Alloys and Compounds, 818 (2020) 152863. https://doi.org/10.1016/j.jallcom.2019.152863

[14] C. Cui, R. Zhang, Y. Zhou, X. Sun, Portevin-Le Châtelier effect in wrought Ni-based superalloys: experiments and mechanisms, Journal of Materials Science and Technology, 51 (2020) 16–31. https://doi.org/10.1016/j.jmst.2020.03.023

[15] M.F. Ashby, D.R.H. Jones, Engineering materials 2: An introduction to microstructures, processing and design, Elsevier, Oxford, 1994, p.150.

[16] J.W. Martin, Precipitation hardening, 2nd ed., Butterworth-Heinemann, Oxford, 1998, p.205.

[17] H. Yuan, W.C. Liu, Effect of the δ phase on the hot deformation behavior of Inconel 718, Materials Science and Engineering: A, 408 (1-2) (2005) 281-289. https://doi.org/10.1016/j.msea.2005.08.126

[18] P. Bai, P. Huo, J. Wang, C. Yang, Z. Zhao, Z. Zhang, L. Wang, W. Du, H. Qu, Microstructural evolution and mechanical properties of Inconel 718 alloy manufactured by selective laser melting after solution and double aging treatments, Journal of Alloys and Compounds, 911 (2022) 164988. https://doi.org/10.1016/j.jallcom.2022.164988

CC BY SA

[19] M. Moiz, The influence of grain size on the mechanical properties of Inconel 718, Master's Thesis, Linköping University, Sweden, 2013.

[20] P. Maj, B. Adamczyk-Cieslak, M. Slesik, J. Mizera, T. Pieja, J. Sieniawski, T. Gancarczyk, S. Dudek, The precipitation processes and mechanical properties of aged Inconel 718 alloy after annealing, Archives of Metallurgy and Materials, 62 (3) (2017) 1695-1702. https://doi.org/10.1515/amm-2017-0259

[21] C. Slama, C. Servant, G. Cizeron, Aging of the Inconel 718 alloy between 500 and 750 °C, Journal of Materials Research, 12 (1997) 2298-2316. https://doi.org/10.1557/JMR.1997.0306

[22] H. Zhang, C. Li, Y. Liu, Q. Guo, Y. Huang, H. Li, J. Yu, Effect of hot deformation on γ″ and δ phase precipitation of Inconel 718 alloy during deformation & isothermal treatment, Journal of Alloys and Compounds, 716 (2017) 65-72. https://doi.org/10.1016/j.jallcom.2017.05.042

[23] F. Theska, K. Nomoto, F. Godor, B. Oberwinkler, A. Stanojevic, S.P. Ringer, S. Primig, On the early stages of precipitation during direct ageing of Alloy 718, Acta Materialia, 188 (2020) 492-503. https://doi.org/10.1016/j.actamat.2020.02.034

[24] C. Kai, D. Jianxin, Y. Zhihao, Creep failure and damage mechanism of Inconel 718 alloy at 800-900 °C, Metals and Materials International, 27 (5) (2021) 970-984. https://doi.org/10.1007/s12540-019-00447-4

[25] K. Pradeep, R.H. Buzolin, M. Domankova, F. Godor, A. Stanojevic, M.C. Poletti, Dynamic recrystallisation in Inconel®718 at creep conditions, Materials Science and Engineering: A, 893 (2024) 146146. https://doi.org/10.1016/j.msea.2024.146146

[26] R.C. Reed, The Superalloys: fundamentals and applications, Cambridge University Press, Cambridge, 2006, p.185.

[27] M.J. Donachie, S.J. Donachie, Superalloys: a technical guide, 2nd ed., ASM International, Materials Park, OH, 2002, p.50.

[28] R.S. Moshtaghin, S. Asgari, The characteristics of serrated flow in superalloy IN738LC, Materials Science and Engineering: A, 486 (1-2) (2008) 376-380. https://doi.org/10.1016/j.msea.2007.09.061

[29] B.S. Rowlands, C. Rae, E. Galindo-Nava, The Portevin-Le Chatelier effect in nickel-base superalloys: Origins, consequences and comparison to strain ageing in other alloy systems, Progress in Materials Science, 132 (2023) 101038. https://doi.org/10.1016/j.pmatsci.2022.101038

[30] X. Zhang, R. Dong, Y. Zhao, D. Liu, L. Yang, H. Hou, Serrated flow behaviors in a Ni-based superalloy, Materials Research Express, 8 (2) (2021) 026515. https://doi.org/10.1088/2053-1591/abe0f2

[31] M. Yang, T. Luo, L. Lei, Y. Jiang, F. Zhao, F. Xu, P. Wang, Unveiling the transition of PLC effects in Haynes 242 superalloy: Role of microstructural states and temperature-dependent deformation mechanisms, Journal of Alloys and Compounds, 1037 (2025) 182286. https://doi.org/10.1016/j.jallcom.2025.182286

[32] P. Rodriguez, Serrated plastic flow, Bulletin of Materials Science, 6 (1984) 653–663. https://doi.org/10.1007/BF02743993

[33] M.T. Pollock, T. Sammy, Nickel-based superalloys for advanced turbine engines: Chemistry, microstructure and properties, Journal of Propulsion and Power, 22 (2) 2006, 361-368. https://doi.org/10.2514/1.18239

[34] C.Y. Cui, C.G. Tian, Y.Z. Zhou, T. Jin, X.F. Sun, Dynamic strain aging in ni base alloys with different stacking fault energy, 12th International Symposium on Superalloys, TMS, 2012, p. 715.

[35] G. Ananthakrishna, Current theoretical approaches to collective behavior of dislocations, Physics Reports, 440 (4–6) (2007) 113–259. https://doi.org/10.1016/j.physrep.2006.10.003

[36] P.K. Pradhan, P.S. Robi, S.K. Roy, Micro void coalescence of ductile fracture in mild steel during tensile straining, Fracture and Structural Integrity, 6 (19) (2012) 51-60. https://doi.org/10.3221/IGF-ESIS.19.05

[37] A. Cui, X. Wang, Y. Cui, Multiscale modelling of precipitation hardening: a review, Journal of Materials Science: Materials Theory, 8 (13) (2024). https://doi.org/10.1186/s41313-024-00066-6

[38] T.J. Oros, K. Son, A.M. Hodge, M.E. Kassner, The high temperature creep and fracture behavior of Inconel 718 produced by additive manufacturing, Scripta Materialia, 251 (2024) 116208. https://doi.org/10.1016/j.scriptamat.2024.116208

[39] R.C. Reed, The Superalloys: Fundamentals and Applications, Cambridge University Press, 2006, p. 185.

UTICAJ HLADNE, TOPLE I VRUĆE DEFORMACIJE NA MIKROSTRUKTURU I MEHANIČKA SVOJSTVA SUPERLEGURE INCONEL 718

Tugay Doğan, Süleyman Gündüz*, Demet Taştemür

Univerzitet Karabuk, Tehnološki fakultet, Karabuk, Turska

Apstrakt

Ova studija sistematski ispituje uticaj precipitacije na mikrostrukturna i mehanička svojstva superlegure Inconel 718 u početnom stanju (as-received), nakon termičke obrade, u stanju maksimalnog starenja i prestarelom stanju. Ispitivanja hladne, tople i vruće deformacije izvedeni su na temperaturama od 25 °C, 400 °C i 800 °C, primenom konstantne brzine deformacije od 5.55×10^{-4} s^{-1}. Rezultati ukazuju na dinamičko starenje usled deformacije tokom tople obrade na 400 °C u svim ispitivanim uslovima. Međutim, na temperaturama iznad 400 °C zabeleženo je značajno smanjenje čvrstoće, praćeno odgovarajućim povećanjem istezanja u većini stanja. Posebno je uočeno anomalno ponašanje kod termički tretiranih uzoraka, koji su pokazali povećanje $Rp_{0,2}$ nakon deformacije na 800 °C. Ovaj rezultat ukazuje na pojavu dinamičke precipitacije tokom tople deformacije u termički tretiranim uzorcima.

Ključne reči: *Superlegure; Dinamičko starenje usled deformacije; Mikrostruktura; Mehanička svojstva*

CC BY SA